JCSE The Journal of Corrosion Science and Engineering

21st Century Corrosion Science

Volume 6 Paper C014

Stress Corrosion Cracking Behaviour of Retrogressed and Reaged 1441 Al-Li-Cu-Mg-Zr Alloy

K. S. Ghosh[1], K. Das[2] and U. K. Chatterjee[2]

[1] *Department of Metallurgical Engineering, National Institute of Technology - Warangal – 506 004, India*. E-mail address: **ghosh@nitw.ernet.in**

[2] *Department of Metallurgical and Materials Engineering, Indian Institute of Technology– Kharagpur - 721302, India*. E-mail address: **ukc@metal.iitkgp.ernet.in**

Abstract

The susceptibility to stress corrosion cracking (SCC) of 1441 Al-Li-Cu-Mg-Zr alloy in the peak aged, over aged and four retrogression and reaged (RRA) tempers has been studied by using slow strain rate technique (SSRT) and constant load technique in 3.5% NaCl, 3.5% NaCl + 0.1M LiCl + 0.3% H_2O_2 and 3.5% NaCl + 0.1M LiCl + 0.7% H_2O_2 solutions under total immersion condition. The studies have shown that 3.5 % NaCl solution has not caused SCC damage, but a small addition of LiCl and H_2O_2 in NaCl solution makes the media conducive to SCC. The peak aged temper has shown the highest susceptibility to SCC, and the over aged temper the lowest. Retrogression and reaging (RRA) treatments of the peak age temper have been found to improve SCC resistance. Optical and SEM observations show that the initiation of stress corrosion cracks has occurred from the base of the pits as well as from the sites of intergranular corrosion, but the crack propagation path is invariably intergranular in all the tempers of the alloy. The improved SCC resistance in the RRA and over aged tempers has been attributed to the enhanced precipitation of anodic phases such as δ and T_1 at the sub-grain boundaries, high angle grain boundaries as well as within the grains that increases uniform attack but minimizes the intensity of intergranular corrosion.

Keywords: Al-Li alloy, Retrogression and reaging, Stress corrosion cracking

1 Introduction

The attractive combination of lighter weight and higher stiffness of Al-Li alloys has rendered them as candidate materials for aerospace applications. The use of Al-Li alloys in place of the most widely used 7xxx series alloys will result in a saving of 8 - 10% structural weight along with an increase of 15% elastic modulus. Al-Li alloys also have superior resistance to fatigue and creep crack growth and higher cryogenic toughness [1]. However, Al-Li alloys have some drawbacks such as the properties are strongly sensitive to processing conditions, unattractive fracture behaviour, especially poor ductility compared to the traditional high strength alloys, high anisotropy of unrecrystallised products as well as susceptibility to environmental induced cracking (EIC) [2,3].

The literature review reveals that there are no consistent trends regarding the effect of aging tempers on EIC of Al-base alloys [4,5]. For example, susceptibility to stress corrosion cracking (SCC) is increased in the Al-Zn-Mg-Cu type alloys in the peak aged (T8) tempers compared to the over aged (T7) tempers [5]. Alloys based on Al-Li-Cu-Zr and Al-Cu-Li-Zr systems are known to exhibit maximum resistance to SC crack initiation in the near peak aged condition, whereas the magnesium containing Al-Li-Cu-Mg-Zr alloys have exhibited maximum resistance to crack initiation in the over aged condition [2,4].

Lumsden and Allen [9] have proposed film rupture and anodic dissolution, rather than hydrogen embrittlement (HE), as the predominant mechanism for the SCC of 1441 alloy. They have reported that the alloy was equally susceptible in all aging conditions. The susceptibility was also potential dependent and there existed a critical potential near the pitting potential below which the alloy was resistant to SCC. They suggested that the critical potential controlled crack propagation but not crack initiation. Thakur and Balasubramaniam [7] have found that 1441 alloy is susceptible to HE, suggesting that hydrogen may play an important role in SCC.

The weight saving and increased stiffness benefits of Al-Li alloys are useful to the aerospace vehicle designers provided the resistance to SCC has been made to improve by suitable heat treatments. The Al-Li-Cu-Mg-Zr alloys are susceptible to SCC in the maximum strength peak aged tempers. The over aged temper has an acceptable SCC resistance [2,4], but lower strength. A relatively new heat treatment process, retrogression and reaging (RRA) treatment is a way to avoid this problem, which makes the heat treatment very attractive to the aerospace industries [8,9]. Commercial retrogression heat treatments are identified by the T77 designation. RRA is a two-stage heat treatment that combines the beneficial effects of both peak aged and over aged tempers. RRA treatments produce microstructures that closely match with those found in the SCC resistant T7 microstructures [10]. Further, dislocations developed during quenching from the solution treatment temperature are annealed out during the retrogression treatment contributing to better SCC performance. Retrogression and reaging (RRA) treatments have also been reported to improve the HE resistance of 1441 alloy in all tempers [7].

The present work discusses the stress corrosion cracking behaviour of a 1441 Al-Li-Cu-Mg-Zr alloy in the peak aged, four retrogression and reaged, and over aged tempers, studied by slow strain arte technique (SSRT) and constant load technique in different SCC media. The SCC behaviour has been explained from the standpoint of microstructural alterations upon RRA treatments.

2 Experimental Procedure

A 1441 (Russian counterpart to 8091 grade) alloy in the sheet form of approximate thickness 2.0 mm has been used for SCC studies. The alloy was cast, homogenized, hot rolled and cold rolled to required thickness. The heat treatment subjected to the 1441 Al-Li alloy was that the cold rolled sheets were solutionized at 530 - 535^{o}C, water quenched, stretched 1.5- 2.5 %, followed by artificial aging at 150^{o}C for 4 hours plus 170^{0}C for 24 hours corresponding to peak aged (T8) temper. The chemical composition (in wt. %) of the 1441 alloy is given in Table 1.

Table 1. Chemical Composition (wt. %) of the1441 Al-Li-Cu-Mg-Zr alloy.

Alloy	Li	Cu	Mg	Zr	Si	Fe	Al
Al	1.90	2.00	0.90	0.09	0.05	0.11	Bal

Initially, retrogression, and retrogression and reaging (RRA) behaviour were studied by hardness measurements. The retrogression treatment of the as–received T8 temper 1441 alloy was carried out at 230 and 270^0C for different time periods varying from 1 to 40 minutes in a small vertical tube furnace in air. The temperature of the tube furnace was maintained within +/- 2^0C. For SCC studies, the RRA schedule was selected in such a way that (i) the retrogression time at a retrogression temperature would cause maximum dissolution of the matrix strengthening δ' precipitates and (ii) reaging the retrogressed state would result in the retention of strength properties in the close proximity to that of the initial as-received peak aged strength. But, it is to be borne in mind that the microstructures of the RRA tempers will definitely differ to that of the as-received peak aged temper as the gross aging time in the RRA temper is almost twice the aging time of the as-received T8 temper. The retrogression and reaging schedule for the as-received specimens is shown schematically in Table 2.

Tensile specimens (transverse to the rolling direction) used for SCC studies were cut from the as-received 1441alloy sheet. Specimen had the dimensions of 20 mm extended gauge length, 4 mm width and 1.8 mm thickness. The surfaces of the gauge portion of the tensile specimen were ground to 100 μm minimum so as to remove the lithium and magnesium depleted and subsurface porosity zones, developed during solutionizing carried out in air [11] and then the gauge portions were polished in emery papers lubricated with kerosene oil up to 600 grits, and finally de-oiled by rinsing in acetone

A CORTEST slow strain rate unit was used for testing at constant elongation rates in air and in 3.5 % NaCl , 3.5% NaCl + 0.1M LiCl + 0.3 H_2O_2 and 3.5% NaCl + 0.1M LiCl + 0.7 H_2O_2 solutions under total immersion condition. All the tests were performed at room temperature at an initial strain rate of 5.5 X 10^{-6} s^{-1}. Stress corrosion cracking studies were also carried out by constant load method in these media under total immersion condition using a Mayer's SC unit, model MK-2, with a lever ratio of 30:1.

Transmission electron microscopy (TEM) studies have been carried out on the peak aged, over aged and some of the RRA tempers for assessing the microstructural changes associated with RRA and aging time. For TEM studies, coupons of approximate dimensions of 15 mm X 15 X 2 mm cut from 1441 sheet was mechanically thinned to a thickness of approximately 100 μm, punched to get 3 mm disc and finally thinned down to perforation using a Fischione twin-jet electropolisher, operating at 25 volts and 2.5 amps, in an electrolyte of composition 30% HNO_3 and 70% CH_3COOH at a temperature of approximately -20^0C. A PHILIPS CW12 TEM was used for the observation of microstructures. The stress corrosion cracks were observed under optical microscope for ascertaining the crack path and fractographic studies were carried out with a Jeol JSM-5800 scanning electron microscope.. X-ray diffraction (XRD) study was carried out for the peak

aged, over aged and various retrogression and reaged tempers, using a Philips PW 1710 diffractometer unit with a cobalt target. Potentiodynamic polarization was carried out by using a computer controlled Meinsberg PS6 potentiostat/galvanostat with an inbuilt software.

Table 2: Rretrogression and reaging (RRA) schedule for the as-received T8 1441 specimens.

Samples for studies	Retrogression temperature and time	Reaging schedule	RRA Temper Designation
Hardness	At 215, 235, 250 and 270^{0}C for 1 to 40 minutes.	Isothermal reaging (IA) at 170^{0}C for 26 corresponding to peak aging temper.	—
SCC, XRD, TEM and electrochemi-cal polarisation	At 230^{0}C for 15 minutes	Isothermal reaging (IA) at 170^{0}C for 26 hours	1441R230IA
		Duplex aging (DA) at 150^{0}C for 36 hours, followed by heating to 190^{0}C at a rate of 5-7 ^{0}C/min and holding for 1 hour at the temperature	1441R230DA
	At 270^{0}C for 5 minutes	Isothermal reaging (IA) at 170^{0}C for 26 hours	1441R270IA
		Duplex aging (DA) at 150^{0}C for 36 hours, followed by heating to 190^{0}C at rate of 5-7 ^{0}C/min and holding for 1 hour at the temperature	1441R270DA

3 Results

3.1 Retrogression and Reaging (RRA) Behaviour

Fig. 1 shows the variation of hardness with retrogression time at retrogression temperatures of 230 and 270^{0}C and with retrogression plus reaging to the peak aging temper. The graphs exhibit the characteristic behaviour of retrogression phenomenon. The hardness versus retrogression time curves show two distinct regions. These is an initial sharp decrease in hardness, attainment of a minimum, followed by a slight increase in hardness after which no further change in hardness values for the maximum retrogression time studied. The trends of the results are in consonance with the results for 7xxx and 8xxx alloy series, obtained by other researchers [12,13]. Further, the curves show that the more the retrogression temperature the more is the drop in hardness values, indicating greater dissolution of the matrix strengthening precipitates.

3.2 Slow Strain Rate Tests (SSRT)

In the slow strain rate tests, the susceptibility to stress corrosion cracking (SCC) has been characterized by various parameters viz. the plastic strain to fracture (ε_p), the

ductility ratio (DR) i.e. the ratio of plastic strain to fracture in environment to that in air ($\varepsilon_{envn}/\varepsilon_{air}$), and the fracture energy (FR) i.e. the area under the plastic region of the stress strain curve in the environment.

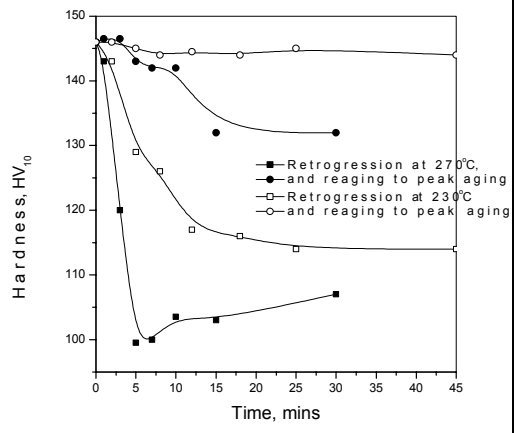

Fig. 1: Retrogression and reaging of 1441 - T8 Alloy

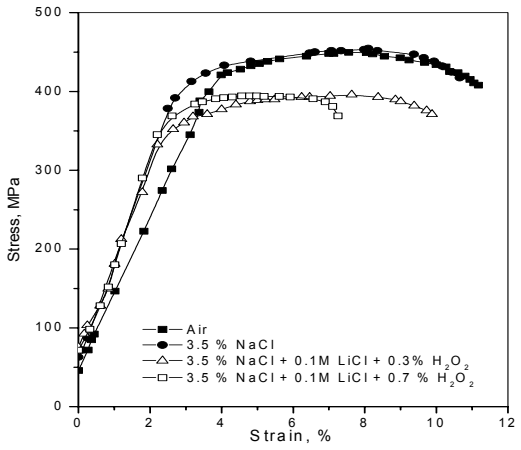

Fig. 2: Representative stress strain curves of 1441R230DA temper.

3.2.1 Effect of Environment on SCC damage

Fig. 2 shows representative stress strain curves of one (1441R230DA) of the RRA tempers studied exhibiting different ductility values in air and in different SCC media. The ductility is maximum in air and least in 3.5% NaCl + 0.1M LiCl + 0.7% H_2O_2 solution. Thus, according to the ductility parameter of indexing SCC susceptibility, the stress strain curves indicate the relative severity of the environments causing SCC damage. Among the test solutions, 3.5% NaCl is least damaging, whereas 3.5% NaCl solution containing LiCl + H_2O_2 are more damaging. The SCC media have also effected a reduction of tensile strength value. A similar effect has also been observed in all the tempers. Table 3 gives the values of ductility ratio (DR) and fracture energy values for all the tempers tested in all the different environments.

Table 3: Ductility ratio of the 1441 alloy of various tempers in different SCC media.

Alloy Temper	3.5% NaCl Solution		3.5% NaCl + 0.1M LiCl + 0.3% H_2O_2 Solution		3.5% NaCl + 0.1M LiCl + 0.7% H_2O_2 Solution	
	Ductility ratio (DR), $\varepsilon_{envn} / \varepsilon_{air}$	Fracture energy, J/Cm^3	Ductility ratio (DR), $\varepsilon_{envn} / \varepsilon_{air}$	Fracture energy, J/Cm^3	Ductility ratio (DR), $\varepsilon_{envn} / \varepsilon_{air}$	Fracture energy, J/Cm^3
1441-T8	0.93	24.05	0.80	21.12	0.36	7.26
1441R270IA	0.88	24.40	0.86	22.34	0.54	10.50
1441R270DA	0.87	23.63	0.83	23.30	0.71	15.00
1441R230IA	0.94	24.60	0.84	23.08	0.59.	12.00
1441R230DA	1.00	27.85	0.85	23.23	0.74	16.00
1441-T7	0.95	22.92	0.90	23.38	0.78	18.03

3.2.2 Effect of RRA Treatment and Aging Time

The retrogressed and reaged tempers have shown higher ductility ratio and fracture energy values indicating better resistance to SCC than the conventional peak aged temper (Table 3).

The average values of plastic strain to fracture ($\varepsilon_{p,\%}$) for all the tempers, tested in all the environments, are shown as bar diagram in Fig. 3. The diagram gives an overall view of the severity of the environment to SCC attack and also the effect of different tempers. For a given environment, the over aged temper has the maximum resistance to SCC, whereas the conventional peak aged temper is most susceptible to SCC. The resistance to SCC attack of the retrogressed and reaged tempers lies in between that of the conventional peak aged and over aged tempers. The bar diagram also indicates that the environments containing LiCl + H_2O_2 are damaging to, whereas the 3.5% NaCl solution has little damaging effect.

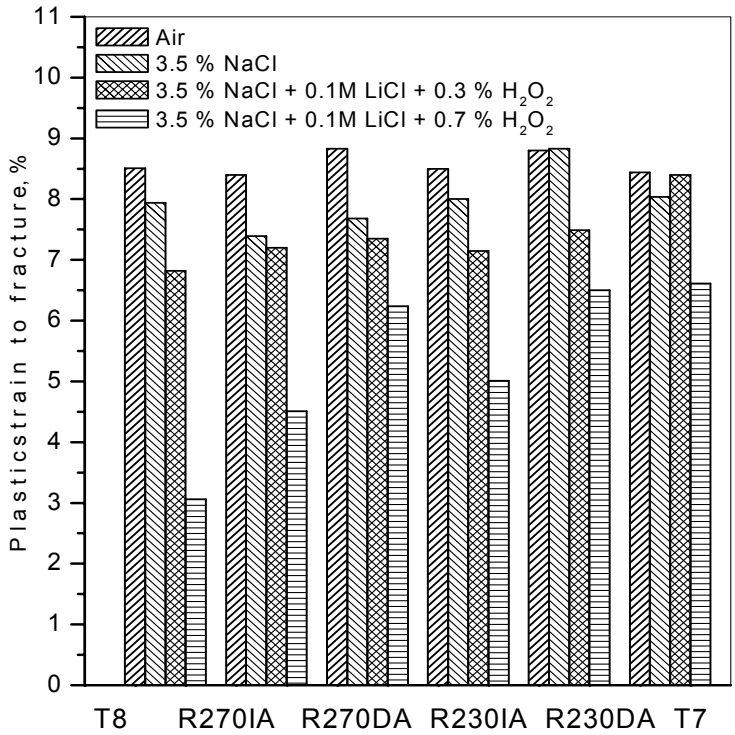

Fig. 3: Plastic strain to fracture of (a) 1441 alloys of various tempers tested in different environments at an initial strian rate of 5.5 X 10^{-6} s^{-1}.

3.3 Constant Load Test

Constant load tests have been carried out to assess the SCC susceptibility of 1441 alloy in the peak aged, retrogression and isothermal and duplex aged, and over aged tempers in 3.5% NaCl + 0.1M LiCl + 0.3% H_2O_2 and in 3.5 NaCl + 0.1M LiCl +

0.7% H_2O_2 solutions at a stress level of 0.92-0.94 of yield stress of the alloy. The test results are shown in Table 4, with time to fracture (t_f) as the SCC susceptibility index.

The time to fracture in all the retrogressed and reaged tempers is more than the time to fracture in the peak aged tempers in both the environments. Thus, the constant load results also indicate an improvement of SCC resistance on retrogression and reaging (RRA) treatments. Further, it is to be mentioned that constant load SCC tests in 3.5% NaCl solution have not caused failure in the 1441 alloy in all tempers, indicating that the solution without any addition of LiCl and H_2O_2 under constant immersion condition is not conducive to SCC.

Table 4: Constant load SCC results of 1441 alloy of various tempers.

1441 alloy Temper	Time of failure (T_f), h	
	3.5 % NaCl + 0.1M + LiCl + 0.3 % H_2O_2 solution	3.5 % NaCl + 0.1M + LiCl + 0.7 % H_2O_2 solution
1441-T8	28, 18	18, 26
1441R270IA	45, 50	24, 22
1441R270DA	18, 38	48, 46
1441R230IA	40, 64	30, 120, 110
1441R230DA	140, 152	34, 50
1441-T7	186^{nf}, 158^{nf}	50, 63

^{nf} : No Failure.

3.4 Mode of Cracking

Stress corrosion (SC) cracking morphology was examined using SEM and optical microscope. Fig. 4(a-f) shows a few representatives SC cracks of 1441 alloy of various tempers tested by SSRT and constant load method in different media. The sources of crack initiation are various. Cracks have initiated either from the pits or from the slip emergence step, or from the intergranularly corroded regions (Fig. 4a). But observations at higher magnification reveal that the crack propagation paths are invariably intergranual and sub-intergranular (Fig 4b, 4c and 4d). The pits are larger in size (Fig. 4e and 4f) and intergranular attack is more in the samples tested by constant load method than those in the samples tested by SSRT. This is due to the fact that in constant load test, samples are exposed for longer time than those tested by SSRT. Further, Fig. 4f shows that the pit base is blunted in the over age temper. This might be the reason for the better SCC resistance of the over aged temper. In samples tested in 3.5 % NaCl solution, numerous pits are visible, but there is no evidence of crack initiation at their base. In retrogressed and reaged and over aged tempers, the sources of crack initiation sites and crack propagation path are the same as those in the peak aged tempers.

3.5 XRD Studies

Fig. 5 shows X-ray diffractograms of peak aged (T8), RRA isothermal (1441R230IA) and duplex aged (1441R270DA), and over aged (T7) tempers using cobalt target. The diffractograms of all the tempers of the alloys show peaks of all the probable phases,

such as α-Al matrix, δ′ (Al_3Li), δ (AlLi), S′ (Al_2CuMg), T_1 (Al_2CuLi) and β′ (Al_3Zr) phases, that would be present in the alloy system. The diffractograms of the samples of the RRA tempers, exhibit the appearance of additional $T_{1(102)}$ peak and other intensified peaks of the T_1 and δ phases.

The appearance of additional $T_{1(102)}$ peak and other intensified peaks of the T_1 and δ phases is due to fact that during retrogression, δ′ (Al_3Li) phase dissolves into solution

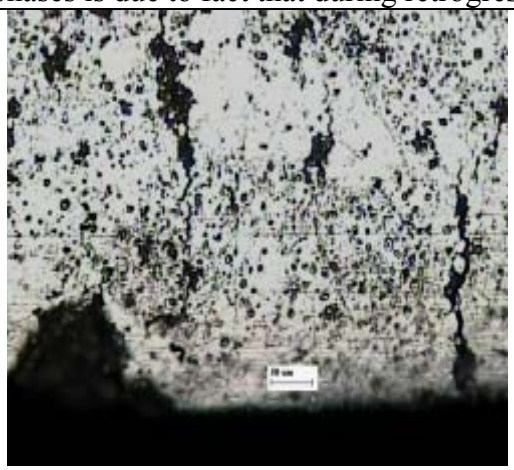

(a)

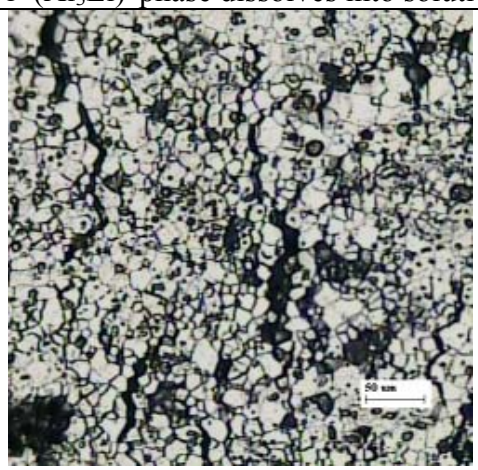

(b)

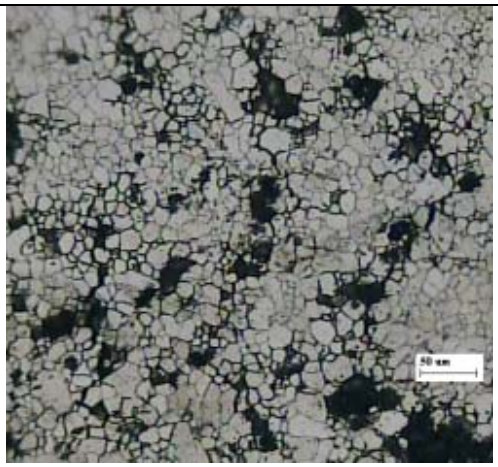

(c)

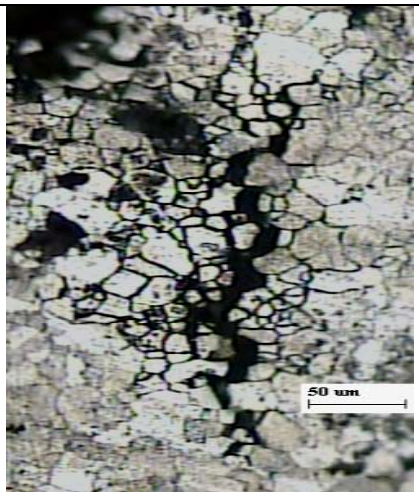

(d)

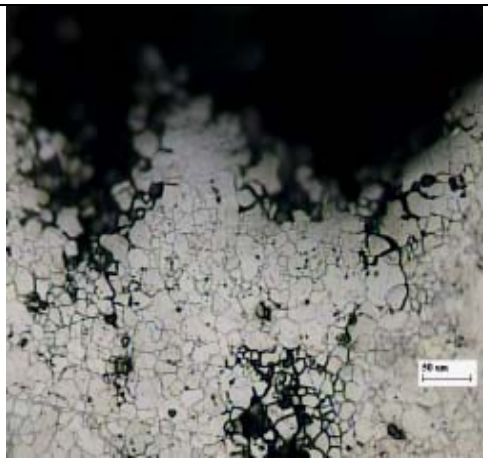

(e)

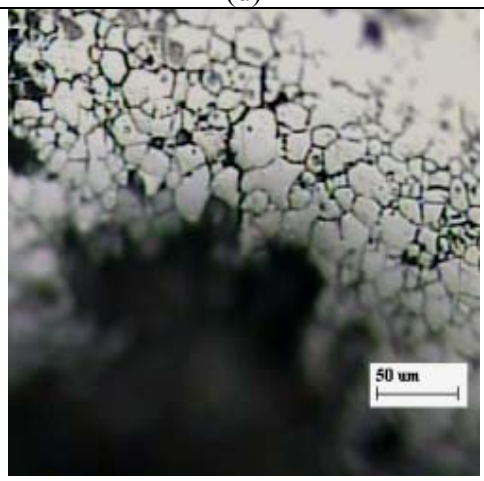

(f)

Fig. 4(a-f): Stress corrosion cracks of (a-b) 1441- T8 temper showing cracks from the base of the pit as well as from other site, but the cracking is intergranular. Crack propagation paths are also intergranular and sub-intergranular in (c) 1441R230IA and (d) 1441770DA retrogressed and reaged tempers. (e) Pits sizes are larger under constant load test and (e) Pit is blunted in the 1441-T7 over aged temper. The SCC media is 3.5% NaCl containing LiCl and H_2O_2.

resulting in an increase of lithium content. This increased lithium content causes nucleation and growth of lithium-bearing phases such as T_1 and δ as well as the growth of the phases that exist in the T8 temper alloy. Hence, in the RRA tempers there are additional or intensified peaks of these phases.

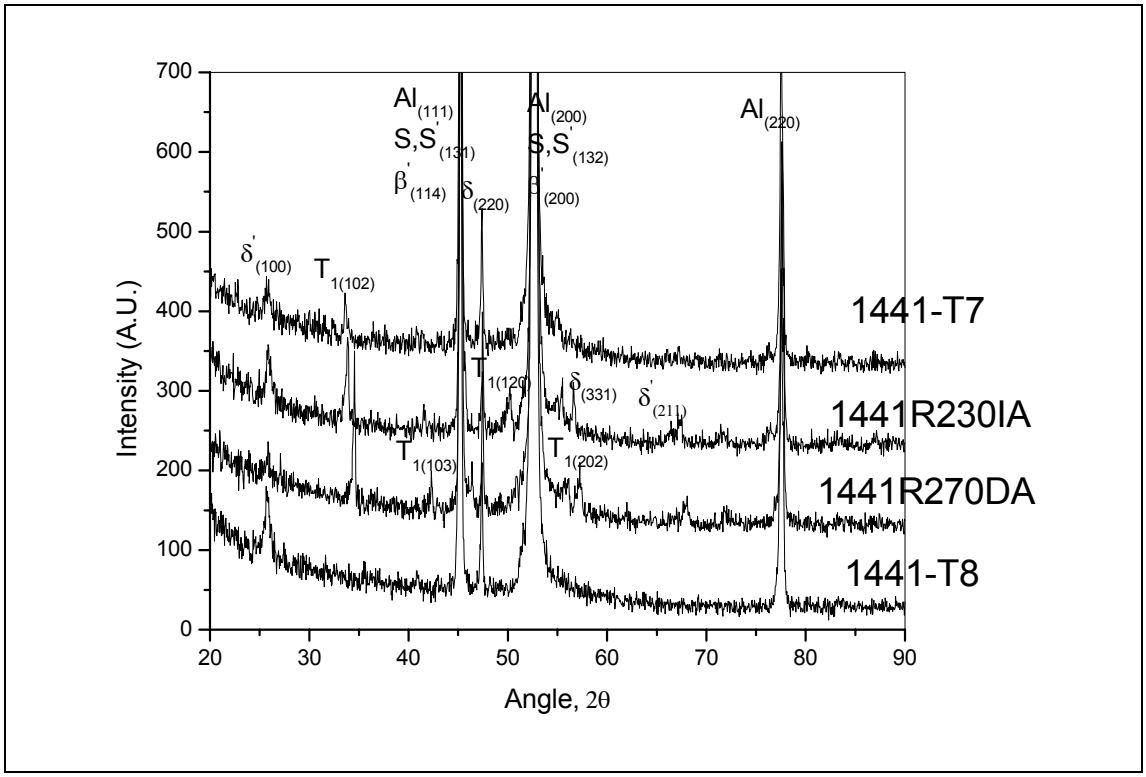

Fig. 5: X-ray diffractograms of the 1441 alloy of various tempers using cobalt target.

3.6 TEM Studies

Some of the representative TEM photomicrographs of the alloy in its various tempers are given in Fig. 6(a-f). Fig. 6a, the bright field image, exhibits grains and grain boundaries containing β' dispersoids, and homogeneously precipitated uniform distribution of fine T_1 and S' phases. In one of the grains in the micrographs, the preferential heterogeneous precipitation of these phases on the dislocations can be seen. Equilibrium δ phase is also visible on the high angle grain boundaries.

Fig. 6(b-c) shows TEM photomicrographs of the retrogressed and duplex reaged (1441R230DA) tempers. Fig. 6b shows clearly the uniform homogeneous distribution of S' phase. Fig. 6c shows the equilibrium δ phase at the high angle grain boundaries and at higher magnification (Fig 6d) these equilibrium δ phase is also visible at the sub-grain boundaries.

Fig. 6(e-f), the TEM micrograph of the 1441-T7 temper shows equilibrium δ precipitates on the high angle grain boundaries, homogeneous uniform distribution of T_1 and S' phases as well as heterogeneous precipitation of these phase along the dislocations [14]. The δ precipitates in this micrograph for the over aged temper are quite larger in size compared to δ precipitates visible in TEM micrographs of the1441-T8 temper (Fig. 6a). The large size of the precipitates on the grain boundaries is expected in the over aged temper. The more the aging time the more is the nucleation and growth of this phase on the grain boundaries. The total aging time in the T7 temper is about four times to that of the T8 temper. Fig. 8f exhibits the densely formed T_1 precipitates and S' phase on the matrix [15]. The dense population of T_1 precipitates on the matrix dictates the condition that over age temper should have very good resistance to SCC for this precipitation hardening aluminium alloy.

3.7 Electrochemical Polarization Studies

Potentiodynamic polarization was carried out for assessing the effect of aging time and retrogression and reaging treatments on the electrochemical behaviour of the 1441 alloy of various tempers. The trends of variation of electrochemical parameters with aging are in consistent with the results of other investigators [4, 16, 17]. Fig. 7 shows the potentiodynamic polarization curves of 1441 alloy in the peak aged, retrogression and reaged, isothermal and duplex, and over aged tempers in 3.5 % NaCl. The shape of the polarization curves is similar for all the tempers. The curves show that the open circuit potential (OCP) has shifted towards more negative values

(a)

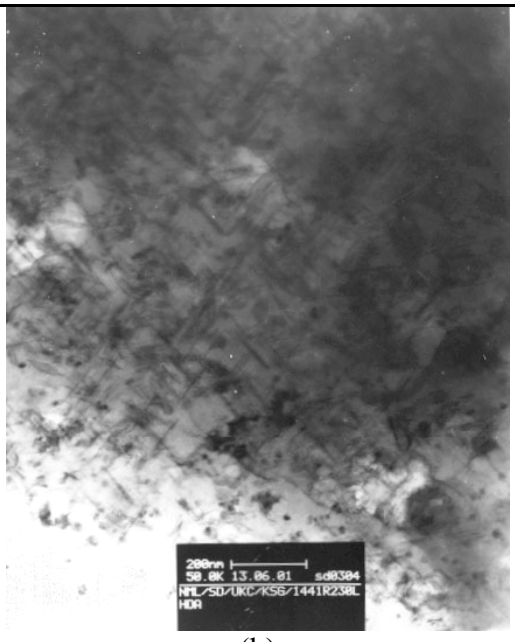

(b)

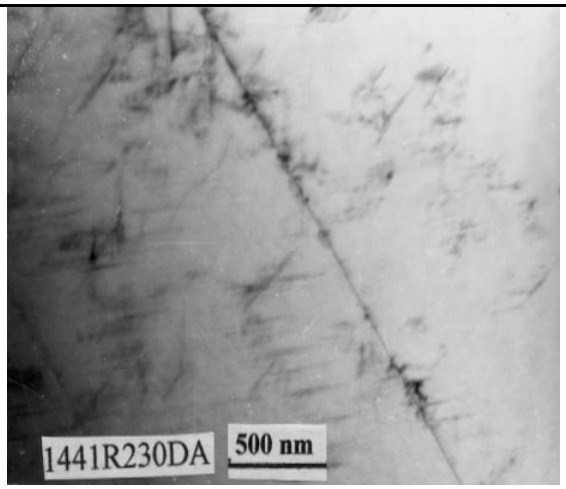

(c)

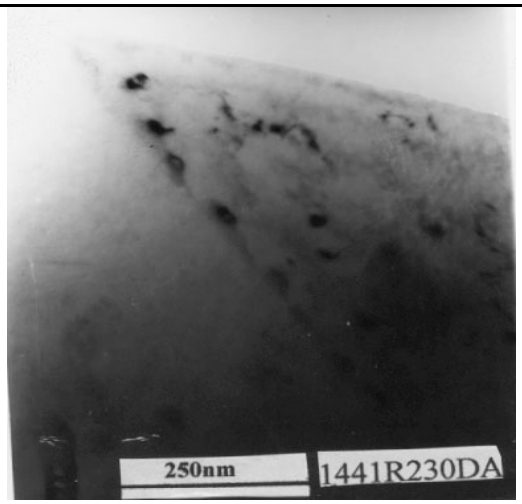

(d)

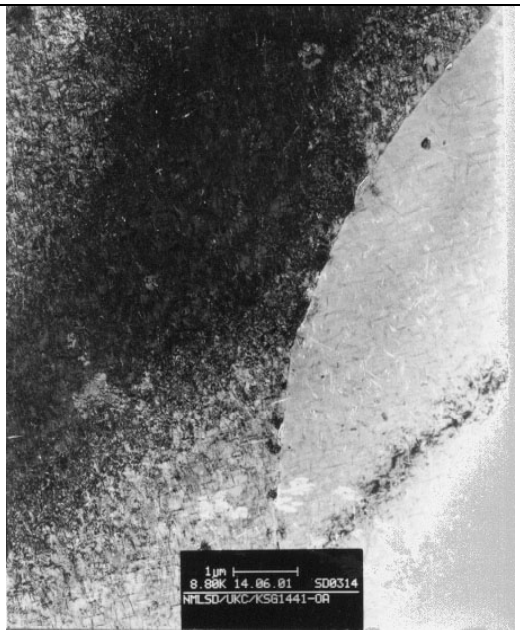

(e)

(f)

Fig. 6(a-f): TEM photomicrographs of the 1441 alloy. (a) 1441T8 temper homogeneous distribution of T_1, S' and β' precipitates in the matrix, and heterogeneous precipitation of T_1 and S' on the dislocations. In 1441R230DA temper (b) uniform and widespread distribution of S' within the matrix, (c) equilibrium δ phase along the high angle grain boundary as well as (d) along the sub-grain boundaries. In 1441-T7 over aged temper (e) exhibiting larger size δ phase along the grain boundary, distribution of T_1, and S' precipitates in the matrix, and heterogeneously on the dislocations and (f) T_1, and S' precipitates densely within the matrix.

with increasing aging time and RRA treatment. The OCP of the over aged temper has the most negative value, whereas the OCP values of the retrogressed and reaged tempers lie in between the OCP values of the over aged and peak aged tempers. It is an established fact that the OCP depends, for a given environment, on the microstructure and the constituent phases. Thus, based on the OCP values, it can be inferred that the microstructure of the retrogression and reaged tempers approaches

the microstructure of the over aged temper. The shifting of the potentials towards anodic direction (i.e. more negative values) with the RRA and aging time can be attributed to the presence of higher amounts of anodic phases such as T_1, δ and S', which has also been confirmed by XRD and TEM studies.

4. Discussion

The initial decrease of hardness with retrogression time (Fig. 1) is due to the preferential dissolution of the shearable coherent matrix strengthening δ' (Al_3Li) precipitates which are no longer stable at the retrogression temperature. Decrease of hardness values on retrogression is also due to the decrease of dislocation density. The minimum in the retrogression curve is indicative of the maximum dissolution of the δ' precipitates. Thereafter, the rate of dissolution and the rate of reprecipitation of the δ'

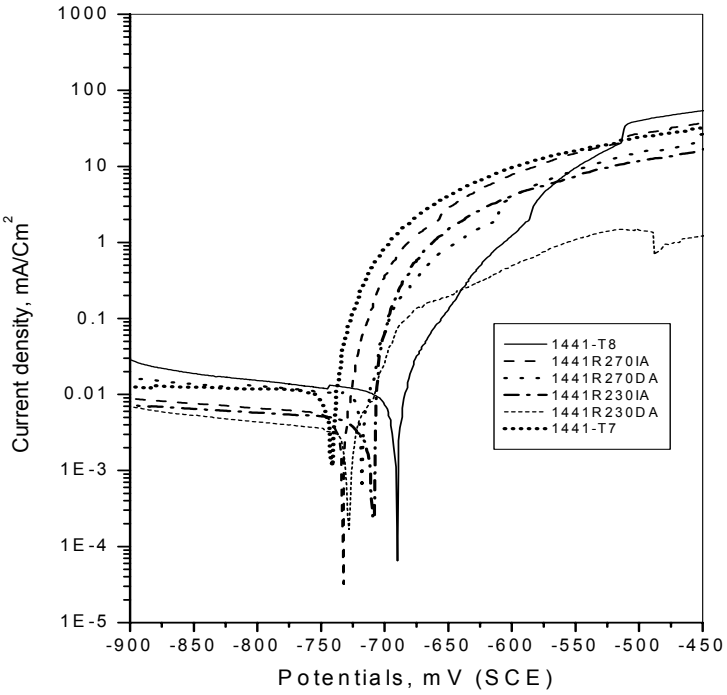

Fig.7: Potentidynamic polarisation curves of 1441 alloy of various tempers in 3.5% NaCl solution.

precipitates might be occurring at the same rate and therefore the hardness remains more or less the same with retrogression time. The decrease of hardness and strength values with increase of retrogression temperatures can be attributed to the fact that higher retrogression temperature causes greater dissolution of the δ' precipitates.

Reaging the retrogressed tempers causes reprecipitation of the matrix strengthening δ' precipitates resulting in an increase of hardness and strength values. The curves indicate that reaging of the samples retrogressed for a short period has led to the regaining of the original peak hardness values. But, with higher retrogression temperature and time, original peak aged hardness values have not been attained on reaging. This is due to the fact that the higher retrogression time leads to a state of

over aging temper [18] and that the retrogression temperature is higher than the peak hardening temperature.

The SCC susceptibility has been found to be low for the alloys in all the tempers under constant immersion condition in 3.5% NaCl solution. The SSRT and constant load methods of SCC testing results show that the addition of small amounts of LiCl and H_2O_2 in 3.5% NaCl solution has made the media conducive to SCC in both the alloys. The absence of SCC in constant immersion condition in NaCl solution has been reported by other investigators as well [2, 19, 20, 21]. The low SCC susceptibility in NaCl solution has been attributed to the depassivating nature of the solution promoting relatively large and blunted pits and blunt grain boundary and subgrain boundary fissures.

The addition of LiCl and H_2O_2 to the 3.5% NaCl solution brings the alloy environment system into a condition of borderline passivity, which is a well-established potential state for SCC in many ferrous alloy systems. The importance of passivation in promoting SCC in aluminium alloys has also been established through the work of many authors. Braun [22] has also reported that a certain amount of lithium ions dissolved during immersions seemed to be required to promote SCC. Buchheit et el [23] has reported that in the 2090 alloy the atmospheric CO_2 absorbed into the crevice solution creates a CO_3^{2-} - Cl^- solution of gradually decreasing pH which allows passivation of the crack walls by the precipitation of $LiAlO_2$. Moran et el [21] and Craig et el [19] have found that either atmospheric CO_2 or the addition of $LiCO_3$ to a NaCl solution promoted SCC of the 2090 alloy. They have established that the precipitation of a salt layer of $LiALO_2$ inside a pit promotes the formation of a sharp fissure with a small, localized anodic area, which is necessary for the nucleation of a stress corrosion crack. Passivation also inhibits crack wall dissolution, maintaining a sharp propagating crack.

The stress-assisted rupture of the passive film normally leads to the local dissolution of the exposed area as it acts as a small anode in contact with a large cathode i.e. the film surface. In the present alloy system, the film rupture exposes an area containing electrochemically anodic T_1 and δ precipitates and it is more likely that the local cell formation leads to a preferential dissolution of these precipitates. The nucleation of crack is produced by pit formation inside which the solution pH goes down the level of 3-4 [2, 24], thus facilitating hydrogen ion reduction as the principal cathodic reaction. It has also been reported [25] that Cu-rich zones act as cathodic depolariser for hydrogen ion reduction, since the hydrogen exchange current density on copper is three times of magnitude higher than that of aluminium. This enhances the anodic current density leading to rapid dissolution. In our studies, the majority of the cracks have been observed to emerge from the base of pits, which could be deemed to have formed at the sites of film breakdown. The lateral growth of the pits has been a later stage development with the intergranular corrosion of the adjacent areas contributing to this growth.

Optical and SEM observations have indicated that stress corrosion cracks have also originated at sites other than the base of pits, such as the regions of intergranular corrosion. The T_1 and δ precipitates are anodic to the matrix [26, 27]. Therefore, there are a lot of microscopic galvanic cells, each consisting of a large cathode and a small anode. The small anode/cathode area ratio results in a high anodic current density,

which provides a large driving force for the dissolution of these phases. Thus, the intergranularly dissolved regions would act as sites for crack initiation in the presence of monotonically increasing stress. Further, the crack initiation is assisted by the propensity for coarse planar slip generated due to the coherent δ' precipitates which causes stress concentration at the grain boundaries.

In the propagation stage, there is a build up of metallic ions at the crack tip, which hydrolyze, resulting in a local acidic condition. This acidic solution inside a crack and the lower potential at the crack tip, as a result of local cell action, increase the H_3O^+ reduction rate to either H_2 gas and/or atomic hydrogen [28]. Accelerated rapid dissolution due to cathodic depolarization may be prevalent in the propagation stage also. At the same time, hydrogen induced cracking may also be operative. However, a visible evolution of gas, presumably H_2, during the test was observed. This is an indication of the difficulty of entry of hydrogen atoms into the metal, apparently due to the restricted reduction of H_3O^+ at the passivated crack walls overlaid with $LiAlO_2$ or $LiCO_3$. [29]. So, localized anodic dissolution can be envisaged as the dominating mechanism during the propagation stage as against a hydrogen induced crack propagation, as suggested by Balasubramanian et el [30] as the dominating mechanism in the SCC of an Al-Li-Cu alloy in 0.5 M NaCl. The difference in operating conditions and alloy chemistry could be the reason for such a difference.

The improvement of SCC resistance in the RRA tempers could be the result of delay in crack initiation and higher resistance of crack propagation compared to that in the peak aged temper. This can largely be attributed to the microstructural changes associated with RRA heat treatment mainly in regard to the size and distribution of the anodic phases δ (AlLi) and T_1 (Al_2CuLi) precipitated within the grains, along the subgrain and grain boundaries as well as of the S' phase.

Retrogression and reaging (RRA) treatments result in the formation of additional equilibrium δ (AlLi) and T_1 phases as indicated by an additional peak of T_1 phase and/or more intense peaks of T_1 and δ phases (Fig. 5, X-ray diffractograms). TEM photomicrographs also exhibit uniform homogeneous distribution of S and T_1 precipitates (Fig. 6b) as well δ phase along the grain boundaries and sub-grain boundaries (fig. 6c and Fig 6d). The higher OCP values observed in potentiodynamic polarization studies (Fig.7) in the RRA tempers compared to those in the peak aged tempers also suggest that RRA treatments have resulted in the precipitation of the anodic S', T_1 and δ phases. The initiation of stress corrosion cracks in this alloy in T8 temper, as already mentioned, is by preferential dissolution of grain boundary δ and T_1 precipitates, due to their anodic nature with respect to the matrix, resulting in the formation of galvanic cells. In the retrogressed and reaged and in the duplex aging tempers, uniform homogeneous distribution of S and T_1 precipitates and more of δ phase along the grain boundaries as well as along the sub-grain boundaries reduce the potential difference for the formation of galvanic cells between the grain and the matrix. Therefore, the tendency of uniform corrosion is more, whereas the propensity of intergranular dissolution is largely reduced. Also in RRA tempers, the homogeneous distribution of S' phase throughout the matrix (Fig. 6b) improves slip homogenization (i.e. minimization of strain localization) by promoting cross-slip, and the low dislocation density [7,10] causes a reduction in stress concentration. All these factors contribute to the improved SCC resistance of the alloys in the RRA tempers. Further, the greater resistance to SCC can also be an outcome of a greater resistance

to stable pit formation. The RRA treatments have resulted in the shifting of the OCP values towards the anodic side. The potential difference between OCP and pitting potential in the RRA and over aged tempers is less compared to that in the peak age tempers, thus reducing the tendency to pit formation.

In the over aged (T7) temper, the aging time is much longer compared to the peak aged and retrogressed and reaged temper. The more the aging time, the more is the precipitation of δ and T_1 phases, on the grain boundaries and on the sub-grain boundaries, which is clearly exhibited in the TEM photomicrographs (Fig. 6e and Fig **6f**). Thus, the potential difference of the galvanic cells formed between the grain and grain boundaries will be small leading to more uniform attack and with low propensity of intergranular corrosion. This in combination with lower strength results in an improved SCC resistance in the T7 temper.

5. Conclusions

1.XRD and TEM studies on the 1441 alloy of various tempers have revealed the presence of all the probable phases, δ′, δ, S′, T_1 and β′ (Al_3Zr) that would be present in the alloy system. Further, XRD studies have exhibited an additional peak and/ or intense peaks of T_1 and δ phases in the RRA tempers. TEM studies have also confirmed the presence of higher amounts of the anodic δ precipitates along the grain boundaries as well as along the sub-grain boundaries and wide spread uniform distribution of T_1 and S′ precipitates.

2.Electrochemical polarization studies have shown that the OCP values of the RRA tempers (T77) lie in between those of the T8 and T7 tempers indicating the presence of higher amounts of these anodic phases in the RRA microstructures.

3.Retrogression treatments given to the 1441-T8 alloy cause a decrease in hardness. Reaging of the lower temperature and short duration retrogressed tempers leads to the regaining of the original T8 hardness.

4.SSRT and constant load methods of SCC testing show that 3.5% NaCl solution is not conducive to SCC susceptibility due to its strong depassivating nature. The addition of a small amount of LiCl and H_2O_2 in 3.5% NaCl, makes the media conducive to SCC in the 1441 alloy by maintaining a condition of passivation required for SCC.

5.The T7 temper has the maximum SSC resistance whereas the T8 has the least SCC resistance. The resistance of RRA tempers lies in between the SCC resistance of the T8 and T7 tempers.

6. Local anodic dissolution plays the dominant role in SCC in this alloy. The higher SCC resistance of the RRA and T7 tempers is attributed to the decreased galvanic effect caused by a uniform distribution of T_1 and δ precipitates within the matrix, and additional precipitation of these precipitates on the grain boundaries as well as on the subgrain boundaries.

6. References

1. J. R. Davis, Davis & Associates, (1998). ASM Specialty Handbook, *Aluminium - lithium alloys*. ASM, Int. Mat. Inf. Society, Ohio, USA.

2. N. J. H. Holroyd, A. Gray, G. M. Scamans and R. Herman (1986). Environment - Sensitive Fracture of Al-Li-Cu-Mg Alloys. *Proc. of the 3rd Int. Conf. on Aluminium-Lithium Alloys III,* The Inst. Metals, London, 310-320.

3. A. Conde, J. J. De Damaborenea (1999). Stress Corrosion Cracking Behaviour of 8090 Al-Li Alloy at 313K. The Effect of Grain Structure (1999). *Corrosion Science*, **41**, 1079 – 1088.

4. A. Gray (1987). Factors Influence the Environmental Behaviour of Aluminium – Lithium Alloys. *Proc of the 4th Int. Conf. on Aluminium-Lithium, Journal de Physique Colloque C3, supplement au no 9, Tome, 48, september*, Paris, C3-891 – C3 904.

5. M. O. Speidel (1975). *Metallurgical Trans A*, **6A**, 631.

6. J. B. Lumsden and A. T. Allen (1988). The Stress Corrosion cracking Behaviour of AlLi Alloy 8090. *Corrsion Sci*., **44**, 527 – 532.

7. C. Thakur and R. Balasubramaniam (1997). Hydrogen Embrittlement of Aged and Retrogressed – reaged Al-Li-Cu-Mg alloys. *Acta mater*., **45**, 1323 - 1132.

8. B. M. Cina and B. Rarish (1974). *Aluminium Industrial Products*, ASM, Pittsburgh.

9. B. M. Cina (1974.). U. S. *Patent 3,856,584*, December 24, 1974.

10. K. S. Ghosh, K. Das and U. K. Chatterjee (2003). Studies on Microstuctural Changes Upon on Retrogression and Reaging Treatment to 8090 Al-Li-Cu-Mg-Zr Alloy. *To be communicated.*

11. S. Fox, H. M. Flower and D. S. McDarmaid (1986). Formation of Solute-depleted Surfaces in Al-Li-Cu-Mg-Zr Alloys and Their Influences on Mechanical Properties. *Proc. of the 3rd Int. Conf. on Aluminium-Lithium Alloys III,* The Inst. Metals, London, 263 – 272.

12. J. K. Park (1988). Influence of Retrogression and Reaging on the Strength and Stress Corrosion Resistance of Aluminium Alloy 7075 – T6. *Mater. Sci. Engg*., **A103**, 223 - 231.

13. Matthew B. Hall and John W. Martin (1994). The effect of Retrogression Temperature on the properties of an RRA (Retrogressed and Reaged) 7150 Aluminium Alloy. *Z. Metallkd*, **85,** 134 - 139.

14. S. Abis, E. Evangelista, P. Mengucci and G. Riontino (1989). Microstructural Evaluation of Al-Li-Cu-Mg-Zr Alloy During Ageing at 160^0C. *Proc. of the 5th Int. Conf. on Aluminium- Lithium Alloys,* 681 – 690.

15. Bi-Ping Huang and Zi-Qiao Zheng (1998). Effects of Li Content on Precipitation in Al-Cu-(Li)–Mg-Ag-Zr Alloys. Scripta Materialia, **38**, 357 - 362.

16. Reboul and P. Meyer (1987). Intergranular and Exfoliation Corrosion Study of Al-Li-Cu-Mg-Zr Alloys. *Proc of the 4th Int. Conf. on Aluminium-Lithium, Journal de Physique Colloque C3, supplement au no 9, Tome, 48, september*, Paris, C3 881 – C3 889.

17. B. Bavarian, J. Becker, S. N. Parikh and M. Zamanzadeh (1989). Localised Corrosion of 2090 and 2091 Al-Li alloys. *Proc. of the 5th Int. Conf. on Aluminium- Lithium Alloys V*, 1227 – 1236.

18. V. Komisarov, M. Talianker and B. Cina (1996). The Effect of Retrogression and Reaging on the Resistance to Stress Corrosion of an 8090 Type Aluminium Alloy. *Materials Science and Engg*, **A221**, 113 – 121.

19. J. G. Craig, R. C. Newman, M. R. Jarrett and N. J. H. Holroyd (1987). Local Chemistry of Stress Corrosion Cracking in Al-Li-Cu-Mg Alloys. *Proc. of the 4th Int. Conf. on Aluminium – Lithium*, C3- 825 – C3 833.

20. G. Disson, M. Reboul, and C. Giaud (1989). A Stress Corrosion Cracking Study of the 2091 Al-Li Alloy. *Proc. of the 5th Int. Conf. on Aluminium – Lithium,* 1261 – 1269.

21. James P. Moron and Glenn E. Stoner (1989). Solution Chemistry Effects on the Stress Corrosion Cracking Behaviour of Alloy 2090 (Al-Li-Cu) and Alloy 2024 (Al-Cu-Mg). *Proc. of the 5th Int. Conf. on Aluminium – Lithium,* 1187 – 1196.

22. R. Braun (1995). Evaluation of the Stress Corrosion Cracking Behaviour of Damage Tolerant Al-Li Sheet using the Slow Strain Rate Testing Technique. *Mater. Sci. Engg*., **A190,** 143 – 154.

23. R. G. Buchheit, F. D Wall, G. E. Stoner and J. P Moran (1995). Anodic Dissolution Based Mechanism for the Rapid Cracking, Pre-exposure Phenomenon Demonstrated by Aluminium – Lithium – Copper Alloys. *Corrosion Science*, **51**, 417 - 428.

24. R. G. Buchheit and G. E. Stoner (1989). The Corrosion Behaviour of the T_1 (Al_2CuLi) Intermetallic Compound in Aqueous Environment. *Proc. of the 5th Int. Conf on Aluminium-Lithium,* 1347 - 1356.

25. E I Meletis (1992). *Parkins Symp. on Fundamental of Stress Corrosion Cracking* (Eds. S. M. Bruemmer, E. I. Meletis, R. H. Jones, W. W. Garberich, F. P. Ford and R. H. Staehle, TMS Publication, 353.

26 P. Niskanen, T. H. Sanders Jr. and J. G. Rinker (1982). *Corrosion Science*, **22**, 283.

27. J. M Sater and T H Sanders (1989). Corrosion Behaviour of Binary Al-Li and Ternary Al-Li-Zr Alloys. *Proc. of the 5th Int. Conf. on Aluminium- Lithium Alloys,* 1217 - 1225

28 C. B. Bargeron, R. C. Benson (1980). Analysis of the gases evolved during the pitting corrosion of aluminium in various electrolytes. *J. Electrochem. Soc*, **127**, 2528.

29. T. D. Burieigh (1991). *Corrosion,* **47**, 89..

30. R. Balasubramanium and D. J. Duquette (1992). *Parkins Symp. on Fundamental of Stress Corrosion Cracking*, 131.